DOE/ET/53088--703

INSTITUTE FOR FUSION STUDIES

DE-FG05-80ET-53088-703 IFSR #703

Studies of Impurity Mode and ITG Mode in Toroidal Plasmas

J.Q. DONG AND W. HORTON
Institute for Fusion Studies
The University of Texas at Austin
Austin, Texas 78712 USA

April 1995

THE UNIVERSITY OF TEXAS

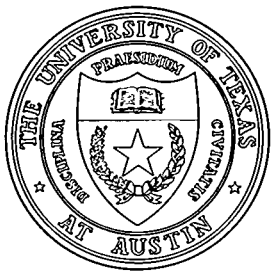

AUSTIN

DISCLAIMER

Studies of impurity mode and ITG mode in toroidal plasmas

J.Q. Dong

Southwestern Institute of Physics, P.O. Box 432, Chengdu, Sichuan 610041

Peoples Republic of China

and

W. Horton

Institute for Fusion Studies, The University of Texas at Austin

Austin, Texas 78712 USA

Abstract

The impurity mode and η_i mode driven by impurity ions with outwardly peaked density profiles, just as it is at the boundary of tokamak plasmas, and the ion temperature gradient, respectively, are studied in high temperature toroidal plasmas. The gyrokinetic theory is applied and finite Larmor radius effects of both hydrogenic and impurity ions are included. It is found that the impurity mode is enhanced by the ion temperature gradient. In addition, the impurity ions with outwardly peaked density profiles are demonstrated to have destabilizing effects on the η_i mode. These two modes are strongly coupled to each other so that it is impossible to distinguish between them when both the driving mechanisms are strong enough to drive the corresponding mode unstable independently. The correlation of the results with nonlinear simulations and the experimental observations are discussed.

PACS Nos.: 52.35.Kt, 52.35.Qz, 52.25.Vy

I. INTRODUCTION

An impurity mode is driven unstable in plasmas where the impurity density profile is outwardly peaked while the hydrogenic ion and electron densities are inwardly peaked, just as it is at the boundary of tokamak plasmas, even without the ion temperature gradient.[1] This mode has been studied in a sheared slab magnetic field under the approximations that the radial wavelength of the eigenmode is much longer than the ion gyroradius ($k_x\rho_i < 1$) and that the response of the impurity ions are fluid-like ($v_i < \omega/k_\parallel$).[2] Recently, the impurity mode is considered to account for the energy transport in plasma periphery and the isotope effect on the energy confinement in tokamak plasmas.[3-10] In most of these early studies of the impurity mode, however, the ion temperature gradient is neglected, that is, the approximation $\eta_i = L_{ni}/L_{Ti} = d\ell n\, T_i/d\ell n\, n_i \sim 0$ is used. The effects of finite ion temperature gradient on the impurity mode need to be studied in detail.

On the other hand, it is widely believed that the ion temperature gradient (ITG or η_i) mode turbulence is responsible for the anomalous energy transport experimentally observed in tokamak plasmas. Extensive investigations have been carried out, experimentally and theoretically, to understand the anomaly of the thermal energy conductivity with ITG turbulence theory in tokamak plasmas.[6-14] Based on the fact that fusion plasmas are not pure single element plasmas composed of electrons and one kind of ions only, say hydrogen or deuterium, rather, they are usually composed of mixture of ionic elements, the effects of second ion species (impurity) on the ITG mode are studied intensively in recent years.[10,15,16]

It is found that impurity ions have stabilizing or destabilizing effects on the ITG mode depending on that the density profile of the impurity ions is outwardly peaked or inwardly peaked. Neither the stabilizing nor destabilizing effect is negligible for the tokamak plasma parameter regimes of interest. The stabilizing effects of impurities on the ITG mode are

studied in detail with toroidal gyrokinetic theory in Ref. 10.

The destabilizing effects of the impurities on the ITG mode, however, have only been studied with simplified models.[10,15,16] A more complete theory with all dynamics of both the hydrogenic ions and impurity ions included has to be applied in such studies in order to make quantitative comparison with experimental observations or to provide reliable benchmark for nonlinear simulations.

Furthermore, the correlation of the impurity mode and the ITG mode has to be studied. One of the interesting issues is to identify the more dangerous one between these two modes for a given set of plasma parameters. This goal can only be achieved with the eigenvalue approach since the initial value method always follows the mode with maximum growth rate without identifying the driving mechanism.

It is first demonstrated explicitly in Ref. 10 that the effects of the impurity ions on the ITG mode depend not only on the dilution of the main ions but also on the density profile and the dynamics of the impurity ions as well, and that the impurity effects on the ITG mode are significant for plasma parameters of interest, so that it is important to take such effects into account when experimental results are analyzed with η_i mode theory. The same integral dispersion equation for low frequency toroidal drift modes is used to study the impurity mode and the η_i mode in this work. Here, the effects of finite η_i on the impurity mode and the negative impurity density gradient on the ITG mode, and the relationship between these two modes are emphasized for toroidal tokamak plasmas.

The remainder of this work is organized as follows. In Sec. II the integral dispersion equation, including second ion species, for toroidal plasmas is presented and explained for completeness. In Sec. III the numerical results are described. The relationship between the results obtained in this work and in earlier papers and experiments are discussed in Sec. IV. Section V is devoted to the conclusions of this study.

II. INTEGRAL DISPERSION EQUATION IN TOROIDAL MAGNETIC FIELD

The integral gyrokinetic equation[9] for the study of low frequency drift modes, such as the impurity mode and η_i mode, is extended to include impurity species in this section. The curvature and magnetic gradient drifts $\omega_D(v_\perp^2, v_\parallel^2, \theta)$ of both hydrogenic and impurity ions are considered. The ballooning representation is used so that the mode coupling due to the toroidicity of the tokamak magnetic configuration is taken into account. The full ion transit $k_\parallel v_\parallel$ and finite Larmor radius effects are retained for both hydrogen and impurity. The ion bouncing is neglected and the electron response is assumed to be adiabatic for simplicity. The integral dispersion equation derived in Ref. 9 is easily written as follows, after being extended to include a second ion species

$$[1+\tau_i(1-f_z)+\tau_z z f_z]\,\widehat{\phi}(k) = \int_{-\infty}^{+\infty} \frac{dk'}{\sqrt{2\pi}} K(k,k')\widehat{\phi}(k'), \tag{1}$$

where

$$K(k,k') = -i\int_{-\infty}^{0} \omega_{*e} d\tau\, \sqrt{2}\, e^{-i\omega\tau}\left[(1-f_z)\frac{\exp\left[-\frac{(k'-k)^2}{4\lambda}\right]}{\sqrt{a}\,(1+a)\sqrt{\lambda}}\right.$$

$$\times\left\{\frac{\omega}{\omega_{*e}}\tau_i + L_{ei} - \frac{3}{2}\eta_i L_{ei} + \frac{2\eta_i L_{ei}}{(1+a)}\right.$$

$$\left.\times\left[1 - \frac{k_\perp^2 + k'^2}{2(1+a)\tau_i} + \frac{k_\perp\, k'_\perp}{(1+a)\tau_i}\frac{I_1}{I_0}\right] + \frac{\eta_i L_{ei}(k-k')^2}{4a\lambda}\right\}\Gamma_0(k_\perp, k'_\perp)$$

$$+ f_z \frac{\exp\left[-\frac{(k'-k)^2}{4\lambda_z}\right]}{\sqrt{a_z}\,(1+a_z)\sqrt{\lambda_z}}\left\{\frac{\omega}{\omega_{*e}} z\tau_z + L_{ez} - \frac{3}{2}\eta_z L_{ez} + \frac{2\eta_z L_{ez}}{(1+a_z)}\right.$$

$$\left.\left.\times\left[1 - \frac{(k_\perp^2 + k'^2)\mu}{2(1+a_z)z^2\tau_z} + \frac{k_\perp\, k'_\perp \mu}{(1+a_z)z^2\tau_z}\frac{I_{1z}}{I_{0z}}\right] + \frac{\eta_z L_{ez}(k-k')^2}{4a_z\lambda_z}\right\}\Gamma_{0z}(k_\perp, k'_\perp)\right] \tag{2}$$

with

$$\lambda = \frac{\tau^2\omega_{*e}^2}{\tau_i a}\left(\frac{\widehat{s}}{q}\epsilon_n\right)^2, \quad \lambda_z = \frac{\tau^2\omega_{*e}^2}{\tau_z a_z \mu}\left(\frac{\widehat{s}}{q}\epsilon_n\right)^2,$$

$$a = 1 + \frac{i2\epsilon_n}{\tau_i}\omega_{*e}\tau\left(\frac{(\widehat{s}+1)(\sin\theta - \sin\theta') - \widehat{s}(\theta\cos\theta - \theta'\cos\theta')}{(\theta-\theta')}\right),$$

$$a_z = 1 + \frac{i2\epsilon_n}{\tau_z z}\omega_{*e}\tau\left(\frac{(\widehat{s}+1)(\sin\theta - \sin\theta') - \widehat{s}(\theta\cos\theta - \theta'\cos\theta')}{(\theta-\theta')}\right),$$

$$\theta = \frac{k}{\widehat{s}k_\theta}, \quad \theta' = \frac{k'}{\widehat{s}k_\theta},$$

$$\Gamma_0 = I_0\left(\frac{k_\perp k'_\perp}{(1+a)\tau_i}\right)\exp\left[-(k_\perp^2 + k'^2_\perp)/2\tau_i(1+a)\right]$$

$$\Gamma_{0z} = I_0\left(\frac{k_\perp k'_\perp \mu}{(1+a_z)\tau_z z^2}\right)\exp\left[-(k_\perp^2 + k'^2_\perp)\mu/2z^2\tau_z(1+a_z)\right],$$

$$k_\perp^2 = k_\theta^2 + k^2, \qquad k'^2_\perp = k_\theta^2 + k'^2,$$

$$\epsilon_n = \frac{L_{ne}}{R}, \quad \eta_i = \frac{L_{ni}}{L_{Ti}}, \quad \eta_z = \frac{L_{nz}}{L_{Tz}}, \quad \tau_i = \frac{T_e}{T_i}, \quad \tau_z = \frac{T_e}{T_z},$$

$$f_z = \frac{zn_{0z}}{n_{0e}}, \quad \mu = \frac{m_z}{m_i}, \quad L_{ei} = \frac{L_{ne}}{L_{ni}}, \quad L_{ez} = \frac{L_{ne}}{L_{nz}}.$$

The quantities k, k' and k_θ are normalized to $\rho_i^{-1} = \Omega_i/v_{ti} = eB/c\sqrt{2T_i m_i}$, x is normalized to ρ_i, and $I_j (j = 0, 1)$ is the modified Bessel function of order j. The symbols with subscript "i" or without stand for the primary ion species (hydrogenic ions) while that with "z" and "e" stand for the second ion species and electrons, respectively, throughout this paper.

In addition, all the symbols have their usual meanings such as the L_n's are the density scale lengths, n_0's are the unperturbed densities, L_T's are the temperature scale lengths, q is

the safety factor, $\hat{s} = rdq/qdr$ is the magnetic shear and $\omega_{*e} = ck_\theta T_e/eBL_{ne}$ is the electron diamagnetic drift frequency. z is the charge number of impurity ions, m's and T's are the species' mass and temperature, respectively. The derivation and detailed explanation of the equation are given in Ref. 9 and not repeated here.

It has to be mentioned before starting to solve Eq. (1) that not all the parameters are independent. This is because the quasineutrality condition holds in the plasmas studied here. This condition requires that

$$L_{ei} = \frac{1 - f_z L_{ez}}{1 - f_z}. \tag{3}$$

Another constraint used in this work is that

$$\eta_z = \frac{\eta_i(\frac{L_{nz}}{L_{ne}} - f_z)}{(1 - f_z)}, \tag{4}$$

which holds under the assumption $T_i(r) = T_z(r)$.

III. NUMERICAL RESULTS

Equation (1) has to be solved numerically and special attention must be paid to the logarithmic singularity at $\tau = 0$ when $k = k'$.[9] The numerical technique for solving such a Fredholm integral equation of the second kind are standard and well documented,[9] and will not be repeated in this work.

The following reference parameters are used in this study unless otherwise stated: $\eta_i = 3, f_z = 0.5, \hat{s} = 1, q = 2.5, \epsilon_n = 0.3, \tau_i = \tau_z = 1, k_\theta \rho_i = 1, L_{ez} = -2$. Hydrogen is considered the primary element except in Fig. 8 where deuterium is used. L_{ei} and η_z are calculated with Eqs. (3) and (4), respectively.

A. Impurity mode

An impurity mode can be driven unstable when there is a second ion species in the plasma and its density peaks opposite to the primary ion and electron densities.[1,2,5] With opposing

density gradients, no ion temperature gradients are needed to drive this instability.

1. L_{ez} variation

The characteristics of the impurity mode are clearly demonstrated in Figs. 1 and 2. Shown in Fig. 1 are the normalized real frequency and growth rate variations with the ratio of density scale lengths $L_{ez} = L_{ne}/L_{nz}$. The specific parameters are $f_z = 0.3, \eta_i = \eta_z = 0, \epsilon_n = 0.1$. Neon with charge number $z = 7$, carbon, and oxygen are considered as impurity. The real frequency of the mode shifts to ion drift direction (being negative) and the growth rate increases when L_{ez} becomes more negative (meaning that the impurity density profile becomes more outwardly peaked). The higher the charge number of the impurity ions, the higher the growth rate and real frequency of the impurity mode. The mode real frequency and growth rate are given in Fig. 2 as a function of L_{ez} for different impurity charge concentration. The same parameters as that in Fig. 1 are used and oxygen is considered to be the impurity. The mode has a higher growth rate for a higher impurity charge concentration f_z when the other parameters are the same, just as expected from a general physics consideration. It is worth pointing out, however, that this conclusion is only meaningful physically when the impurity charge concentration f_z is not too high. The reason is that the density profile of the impurity ions are outwardly peaked, ($L_{nz} < 0$) and the density profiles of the primary ions and the electrons are inwardly peaked ($L_{ne} > 0, L_{ni} > 0$). The ion density scale length has to be unrealistically small in order to satisfy the quasineutrality condition if the impurity charge concentration is too high. For example, $L_{ei} = 28$ for $f_z = 0.9$ according to Eq. (3) if $L_{ez} = -2$.

2. Toroidicity effect

The normalized real frequency and growth rate of the impurity mode versus the toroidicity parameter $\epsilon_n = L_{ne}/R$ are given in Fig. 3 for $\eta_i = \eta_z = 0, q = 2.5, 3.5$, and 4.5. Carbon

(C) and oxygen (O) are considered. It is shown that the normalized real frequency (in the ion direction) increases with the toroidicity parameter ϵ_n linearly, and is independent of the impurity ion species. The maximum growth rate appears around $\epsilon_n = 0.3$ for all the situations considered here. The mode growth rate is higher for a higher q value. Oxygen impurity may drive stronger instability than carbon impurity does for the same safety factor $q = 2.5$.

3. Ion temperature gradient effect

Shown in Fig. 4 are the normalized real frequency and growth rate of the impurity mode versus the ion temperature gradient parameter η_i. The parameters $\hat{s} = 0.5, k_\theta \rho_i = 0.65, 1,$ and 1.45 are used. The real frequency is always negative for the η_i values from -1 to 3 and increases (in the ion direction) with the increase of η_i. A positive η_i has a destabilizing effect on the impurity mode while a negative η_i is a stabilizing factor. A negative η_i means that the primary ion temperature profile is outwardly peaked since electron and impurity ion density profiles are assumed to be inwardly and outwardly peaked, respectively, and the primary ion density profile cannot be outwardly peaked anymore according to the quasineutrality condition. This physical consideration will be discussed again in Sec. IV.

4. $k_\theta \rho_i$ spectrum

The $k_\theta \rho_i$ spectrums of the impurity mode are given in Fig. 5 for $\eta_i = 0, 1,$ and 2. Carbon is considered as impurity, and $\hat{s} = 0.5$ is used. The real frequency increases with $k_\theta \rho_i$ monotonously while the growth rate has a peak around $k_\theta \rho_i = 0.8$.

The peak of the growth rate shifts to small $k_\theta \rho_i$ slightly when η_i increases. The ion temperature gradient (η_i) has destabilizing effects on the impurity mode over all the $k_\theta \rho_i$ region studied here.

B. Ion temperature gradient mode

The numerical results for ion temperature gradient (ITG) driven mode in toroidal plasmas with outwardly peaked impurity density profile are presented in this subsection. The results for plasmas in shearless slab and sheared slab magnetic fields can be found in early studies.[2,10]

1. Impurity charge concentration f_z effects

Shown in Fig. 6 are the variations of the ITG mode real frequency and growth rate with the impurity charge concentration f_z for $k_\theta \rho_i = 0.65, 1$, and 1.45. Carbon is considered as impurity. The real frequency and growth rate both increase monotonously with the impurity charge concentration f_z. This is significantly different from the results for the plasmas of $L_{ez} > 0$ where the real frequency decreases with f_z and the growth rate has a minimum close to $f_z = 0.5$ (see Fig. 4 of Ref. 10). This difference may be due to the fact that $L_{ei} = L_{ez} = 1$ is assumed in Ref. 10 so that $L_{ni} = L_{nz} = L_{ne}$ are constant when f_z increases. Here, however, L_{ni} has to decrease in order to satisfy the quasineutrality condition when f_z increases, just as discussed for Fig. 2. It may be concluded from these results that primary ion density gradient may have a destabilizing effect on ITG mode in plasmas with negative impurity ion density gradient.

2. L_{ez} variation

The variations of ITG mode real frequency and growth rate with the ratio of the electron density scale length over the impurity density scale length $L_{ez} = L_{ne}/L_{nz}$ are given in Fig. 7. The parameters are $\eta_i = 3.3, \hat{s} = 0.83, q = 1.5, \epsilon_n = 0.56, f_z = 0.1, 0.2$, and 0.3. Neon with charge number $z = 7$ is considered as impurity. The results are similar to that given in Figs. 1 and 2 for the impurity mode except that the ITG mode is unstable while impurity mode becomes stable when L_{ez} reaches 0. It is clearly demonstrated here that a negative and a

positive impurity density gradient (outwardly and inwardly peaked impurity density profile) has destabilizing and stabilizing effects on the ITG mode in tokamak plasmas, respectively. Impurity ions with flat density profile ($L_{ez} = 0$) have a stabilizing effect on the mode due to the dilution of the main ions. This result has been obtained in an earlier study[15] with local approximation and is repeated with full integral dispersion approach in this work.

3. $k_\theta \rho_D$ spectrum

The $k_\theta \rho_D$ spectrums of the ITG mode in a deuterium and carbon mixture plasma are presented in Fig. 8 for $f_z = 0.3$, $L_{ez} = -2, -1$, and 1. The mode rotates in the ion drift direction and the frequency increases with the decreasing of L_{ez}. The maximum growth rate appears at $k_\theta \rho_i \sim 0.55$ for $L_{ez} = 1$ while it shifts to $k_\theta \rho_i \sim 0.8$ for $L_{ez} = -2$. The maximum growth rate for $L_{ez} = -2$ is 6 times that for $L_{ez} = 1$ and the unstable region of $k_\theta \rho_i$ for the former is much broader than that for the latter. The impurity ions with density peakness being opposite to that of the primary ions and the electrons have strong destabilizing effects on the ITG mode all over the $k_\theta \rho_i$ region of interest.

IV. DISCUSSION

It has been reported[4,16] that the impurity mode and the η_i mode can both be unstable simultaneously and there exist two unstable modes for some plasma parameters. These results are obtained with fluid or local approximation in a slab geometry. The more comprehensive kinetic calculations carried out in the present work yield one unstable mode only. In order to make a comparison with the earlier results, the local approximation is made to reduce Eq. (1) to the following formula in a toroidal magnetic configuration,

$$1 + \tau_i(1 - f_z) + \tau_z\, z\, f_z + i \int_{-\infty}^{0} \omega_{*e} d\tau\, 2e^{-i\omega\tau} \left[(1 - f_z)\, \frac{\exp[-(k_\parallel v_i \tau)^2/4a]}{\sqrt{a}\,(1+a)} \left\{ \tau_i\, \frac{\omega}{\omega_{*e}} \right.\right.$$

$$+ 1 - \tfrac{3}{2}\eta_i L_{ei} + \frac{2\eta_i L_{ei}}{(1+a)} F_0 + \eta_i L_{ei} + \frac{2\eta_i L_{ei}}{1+a)} F_0 + \eta_i L_{ei}\left[\frac{1}{2a} - \frac{1}{4a^2}(k_\parallel v_i \tau)^2\right]\Bigg\}\Gamma_0(k_\perp)$$

$$+ f_z \frac{\exp\left[-(k_\parallel v_z \tau)^2/4a_z\right]}{\sqrt{a_z}(1+a_z)}\Bigg\{\frac{\omega}{\omega_{*e}}\tau_z z + L_{ez} - \tfrac{3}{2}\eta_z L_{ez} + \frac{2\eta_z L_{ez}}{(1+a_z)} F_{0z}$$

$$+ \eta_z L_{ez}\left[\frac{1}{2a_z} - \frac{1}{4a_z^2}(k_\parallel v_z \tau)^2\right]\Bigg\}\Gamma_{0z}(k_\perp)\Bigg] = 0 \qquad (5)$$

where

$$F_0 = 1 - \frac{k_\perp^2}{(1+a)\tau_i}\left(1 - \frac{I_1}{I_0}\right),$$

$$\Gamma_0(k_\perp) = I_0\left(\frac{k_\perp^2}{(1+a)\tau_i}\right)\exp\left[-k_\perp^2/\tau_i(1+a)\right],$$

$$F_{0z} = 1 - \frac{k_\perp^2 \mu}{(1+a_z)\tau_z z^2}\left(1 - \frac{I_{1z}}{I_{0z}}\right),$$

$$\Gamma_{0z}(k_\perp) = I_0\left(\frac{k_\perp^2 \mu}{(1+a)\tau_z z^2}\right)\exp\left[-\frac{k_\perp^2 \mu}{\tau_z z^2(1+a_z)}\right],$$

and v_i and v_z are the thermal velocity of the hydrogenic and impurity ions, respectively.

The numerical results from Eq. (5) are given in Fig. 9 for the plasma parameters: $\eta_i = 7, f_z = 0.5, \hat{s} = 0.83, q = 1.5, L_{ei} = L_{ez} = 1, \epsilon_n = 0.56, \tau = \tau_z = 1, k_\parallel = 1/qR, z = 10$, and $m_z/m_i = 20.18$. For $0.35 \lesssim k_\theta \rho_i \lesssim 0.6$ there are two unstable modes while for $0.95 \gtrsim k_\theta \rho_i \gtrsim 0.6$ or $k_\theta \rho_i \lesssim 0.35$ one unstable root is found only. These results are confirmed with the Nyquist technique. The mode with higher growth rate rotates in the ion diamagnetic drift direction and is the conventional ITG mode of the primary or the impurity ions. Another mode with lower growth rate rotates in the electron direction. It is shown in Fig. 9(c) (the solid line) that this mode becomes stable when f_z approaches 0 or 1, which means that this mode is driven by the interaction between the primary and the impurity ions. This mode may only be unstable in a small regime of $k_\parallel$ value so that it is completely suppressed in the calculations with the integral equation.

An important issue has been left untouched although the impurity and ITG modes have been enormously investigated. That is, which mode, the impurity mode or the ITG mode, is more dangerous for plasmas with both a finite ion temperature gradient and a negative impurity density gradient. Efforts are made to address this issue in the present work.

By comparing the results in Fig. 4 for $\eta_i = 3$ with that in Fig. 6 for $f_z = 0.5$, it is easy to find that they are the same for same $k_\theta \rho_i$. This is not what had been expected before it was reached. Efforts have been made to find a second mode for the same set of parameters and failed. The impurity mode and the η_i mode are strongly coupled to each other so that it is impossible to distinguish between them when both driving mechanisms are strong enough to drive the corresponding mode unstable independently. In other words, only one unique mode is driven unstable by the combination of these two driving forces. This is good for nonlinear simulations, which usually solve an initial value problem and can only follow the mode with maximum growth rate, since it is not necessary to worry about a second mode when such simulations are carried out.

One of the major discrepancies between the conventional drift wave theories and experiments on the anomalous thermal transport in tokamak plasmas is that the energy conductivity in the periphery is higher experimentally and lower theoretically than that in the core, respectively.[8] Such discrepancy is demonstrated once again by recent comprehensive comparisons[14] of nonlinear toroidal turbulence simulations with experiment where theoretical χ_is increase in the radial direction until $r/a \sim 0.8$ to the best. The simulations cannot provide satisfactory comparison beyond. Impurity mode has been proposed to overcome this theoretical obstacle.[1,3,5] It is demonstrated in this work that the impurity mode and the ITG mode are strongly coupled to and enhance each other. The coupled mechanisms of impurity density gradient and ion temperature gradient, studied here in detail, may provide a possible solution for this problem.

V. CONCLUSIONS

The impurity mode driven unstable by the presence of impurity ions with the peakness of the density profile opposite to that of primary ions and electrons is studied in toroidal magnetic configuration. The real frequency and growth rate are calculated for a wide region of such plasma parameters as $L_{ez}, f_z, \varepsilon_n, q, \widehat{s}$, and $k_\theta \rho_i$, and for carbon, oxygen, and neon impurities. It is demonstrated that the mode is rather robust and that the growth rate of the mode is higher in a plasma with impurity of high charge number than that in a plasma with low charge number impurity. This is in line with the experimental observations that wall condition of the vacuum vessel, aimed at reducing high z impurities in tokamak plasmas, lead to better plasma confinement if the impurity mode is applied to account for (at least, partial) anomalous energy diffusivity measured in experiments. The effects of the ion temperature gradient on the impurity mode are demonstrated to be stabilizing and destabilizing for $\eta_i < 0$ and $\eta_i > 0$, respectively.

The ion temperature gradient (or η_i) mode is studied in the presence of a second ion species (impurity) in tokamak plasmas. The impurity species has stabilizing and destabilizing effects on the ITG mode for $L_{ne}/L_{nz} > 0$ and $L_{ne}/L_{nz} < 0$, respectively.

The impurity mode and the η_i mode are strongly coupled to and enhance each other. It is impossible to distinguish between them in plasmas with $L_{ne}/L_{nz} < 0$. In such plasmas the threshold value η_{ic} for the instability is much lower than it is in plasmas with $L_{ne}/L_{nz} > 0$. The instability is possible even for $\eta_i \lesssim 0$ in the former while the mode is unstable only for $\eta_i > \eta_{ic} \simeq 1$ in the latter. The combined mechanisms of the impurity density gradient and the ion temperature gradient provide 5 times higher growth rate than the pure ITG mode does, and may be a solution for the theoretical understanding of the diffusivity in the periphery ($r/a > 0.8$) of tokamak plasmas.

Acknowledgments

The authors would like to thank Drs. T. Tajima, F.L. Waelbroeck, W. Dorland, and M. Kotschenreuther for useful discussions. One of the authors (JQD) would like to thank the faculty and staff at the Institute for Fusion Studies at The University of Texas at Austin for their hospitality.

This work was supported in part by the U.S. Department of Energy contract No. DE-FG05-80ET-53088 and in part by the Southwestern Institute of Physics, China.

REFERENCES

[1]B. Coppi, H.P. Furth, M.N. Rosenbluth, and R.Z. Sagdeev, Phys. Rev. Lett. **17**, 377 (1966).

[2]W.M. Tang, R.B. White, and P.N. Guzdar, Phys. Fluids **20**, 167 (1980).

[3]B. Coppi, in *Plasma Physics and Controlled Nuclear Fusion Research* (International Atomic Energy Agency, Vienna, 1991) Vol. 2, p. 413.

[4]S. Migliuolo, Nucl. Fusion **33**, 3 (1993).

[5]J.Q. Dong, W. Horton, and W. Dorland, Phys. Plasmas **1**, 3635 (1994).

[6]S.D. Scott, *et al.*, in *Plasma Physics and Controlled Nuclear Fusion Research* (International Atomic Energy Agency, Vienna, 1991) Vol. 1, p. 235.

[7]M.C. Zarnstorff, *et al.*, in *Plasma Physics and Controlled Nuclear Fusion Research* (International Atomic Energy Agency, Vienna, 1991) Vol. 1, p. 109.

[8]W. Horton, D. Lindberg, J.Y. Kim, J.Q. Dong, G.W. Hammett, S.D. Scott, and M.C. Zarnstorff, Phys. Fluids B 4, 952 (1992).

[9]J.Q. Dong, W. Horton, and J.Y. Kim, Phys. Fluids B 4, 1867 (1992).

[10]J.Q. Dong, W. Horton, and X.N. Su, in *Ion Temperature Gradient-Driven Turbulent Transport*, eds. W. Horton, A. Wootton, and M. Wakatani, (American Institute of Physics Conference Proceedings, January, 1994), p. 486.

[11]W.W. Lee, S.E. Parker, R.A. Santoro, and J.C. Cummings, *ibid*, p. 213.

[12]T. Tajima, Y. Kishimoto, M.J. LeBrun, M.G. Gray, J.Y. Kim, W. Horton, V. Wong, and M. Kotschenreuther, *ibid*, p. 255.

[13]Y. Kishimoto, T. Tajima, M.J. LeBrun, W. Horton, J.Y. Kim, J.Q. Dong, F.L. Waelbroeck, S. Tokuda, M. Kawanobe, and T. Fukuda, IAEA-CN-601D-2-II-3, Seville, Spain, 26 September–1 October, 1994.

[14]W. Dorland, M. Kotschenreuther, M.A. Beer, G.W. Hammett, R.E. Waltz, R.R. Dominguez, P.M, Valanju, W.H. Miner, Jr., J.Q. Dong, W. Horton, F.L. Waelbroeck, T. Tajima, and M.J. LeBrun, *ibid*, D-P-I-6.

[15]R.R. Dominguez, Nucl. Fusion **32**, 2063 (1991).

[16]A. Jarmén and M. Frödjh, Phys. Fluids B **5**, 4015 (1993).

FIGURE CAPTIONS

FIG. 1. Normalized real frequency (a) and growth rate (b) of the impurity mode versus the ratio of density scale lengths $L_{ez} = L_{ne}/L_{nz}$. The specific parameters are $\eta_i = \eta_z = 0$, $f_z = 0.3$, and $\varepsilon_n = 0.1$. Carbon, neon with ionization state of $z = 7$, and oxygen are considered as impurity.

FIG. 2. The same as that in Fig. 2 but for oxygen impurity and different impurity charge concentration f_z.

FIG. 3. Normalized real frequency (a) and growth rate (b) of the impurity mode versus ε_n for $\eta_i = \eta_z = 0, q = 2.5, 3.5$, and 4.5. Carbon and oxygen impurities are considered.

FIG. 4. Normalized real frequency (a) and growth rate (b) of the impurity mode versus η_i for $\hat{s} = 0.5$, $k_\theta \rho_i = 0.65, 1$, and 1.45. Carbon impurity is considered.

FIG. 5. Normalized real frequency (a) and growth rate (b) of the impurity mode versus $k_\theta \rho_i$ for $\eta_i = 0, 1$, and 2. Carbon impurity is considered and $\hat{s} = 0.5$.

FIG. 6. Normalized real frequency (a) and growth rate (b) of the η_i mode versus the impurity charge concentration f_z for $k_\theta \rho_i = 0.65, 1$ and 1.45, and carbon impurity.

FIG. 7. Normalized real frequency (a) and growth rate (b) versus the ratio of density scale lengths $L_{ez} = L_{ne}/L_{nz}$ for $\eta_i = 3.3, \hat{s} = 0.83, q = 1.5, \varepsilon_n = 0.56, f_z = 0.1, 0.2$, and 0.3. Neon impurity* of ionization state $z = 7$ is considered.

FIG. 8. Normalized real frequency (a) and growth rate (b) of the η_i mode versus $k_\theta \rho_D$ in deuterium and carbon mixture plasmas of $f_z = 0.3, L_{ez} = -2, -1$, and 1.

FIG. 9. The numerical results from the local approximation, (a) the real frequency versus $k_\theta \rho_i$, (b) the growth rate versus $k_\theta \rho_i$, and (c) the growth rate versus f_z. The parameters are $\eta_i = 7, \hat{s} = 0.83, q = 1.5, L_{ei} = L_{ez} = 1, \epsilon_n = 0.65, \tau = \tau_z = 1, z = 10, m_z/m_i = 20.18$.

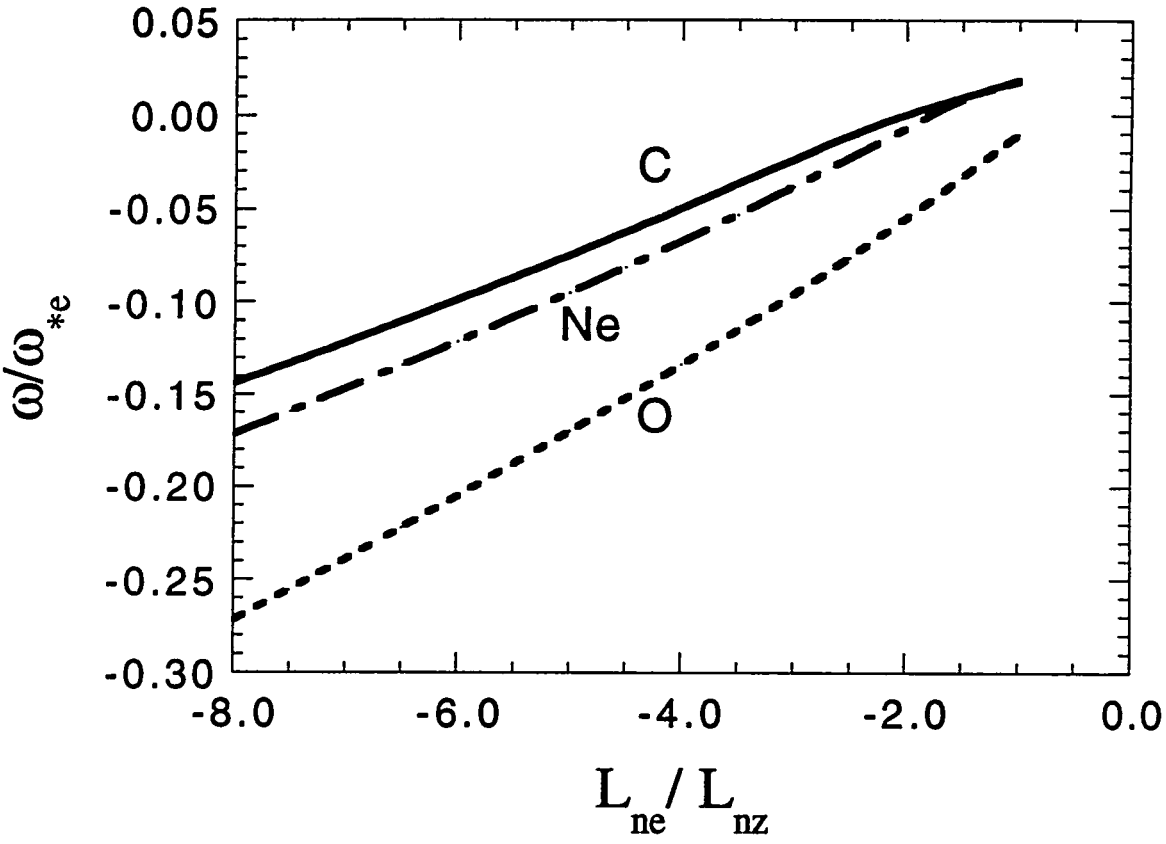

Fig.1(a)

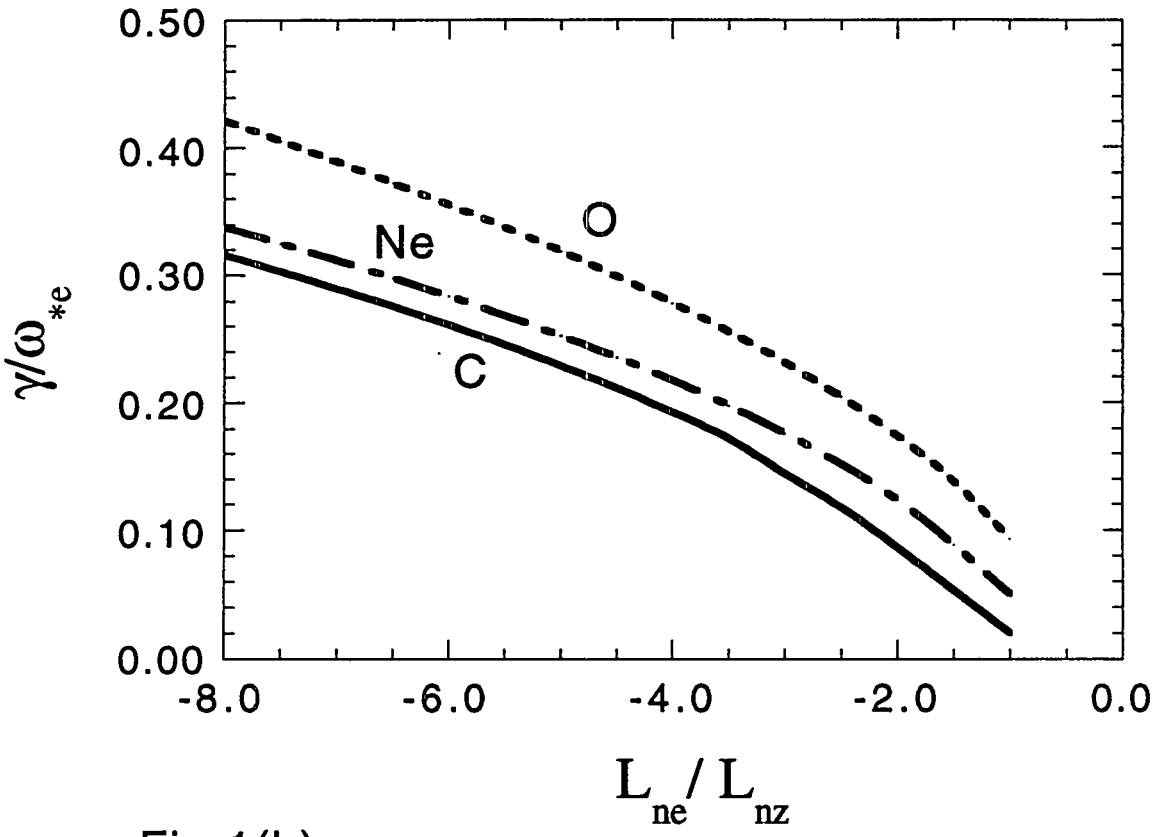

Fig.1(b)

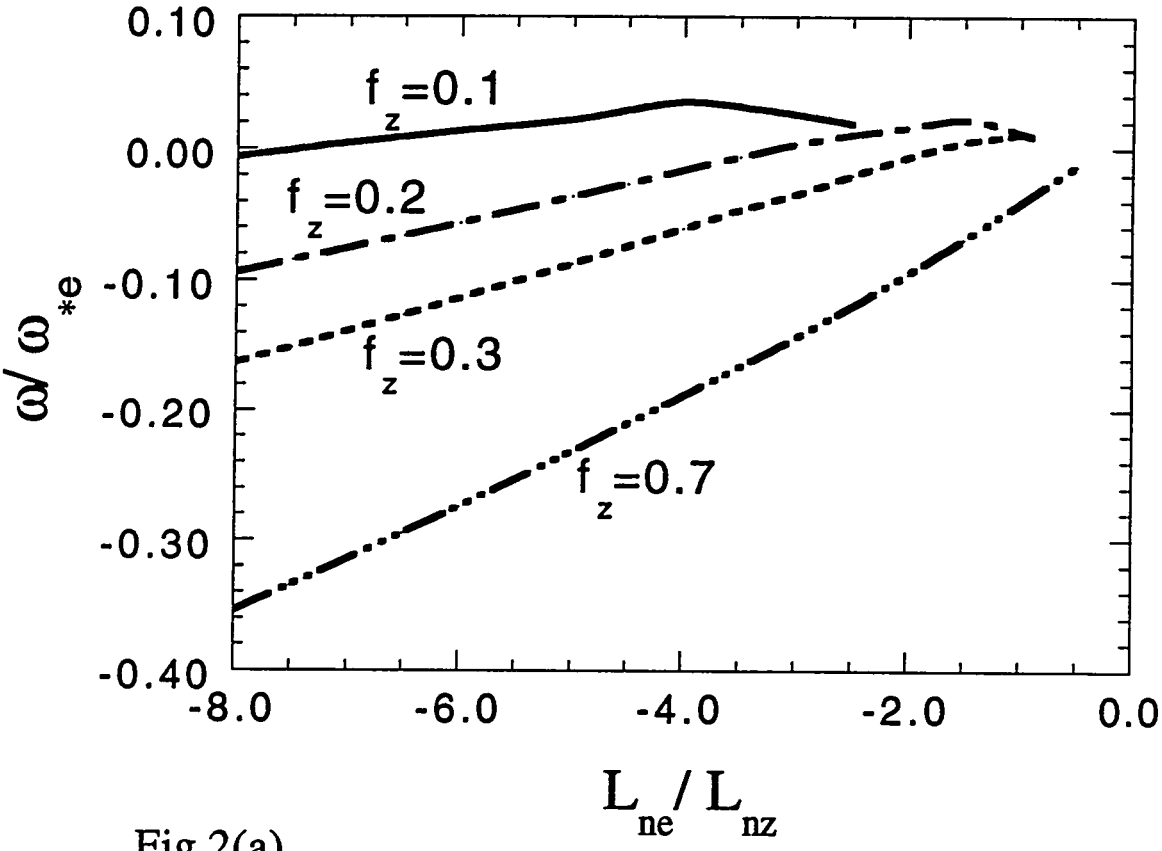
0.10
0.00
-0.10
-0.20
-0.30
-0.40
-8.0
-6.0
-4.0
-2.0
0.0
ω/ω*e
f z=0.1
f z=0.2
f z=0.3
f z=0.7
L ne / L nz

Fig.2(a)

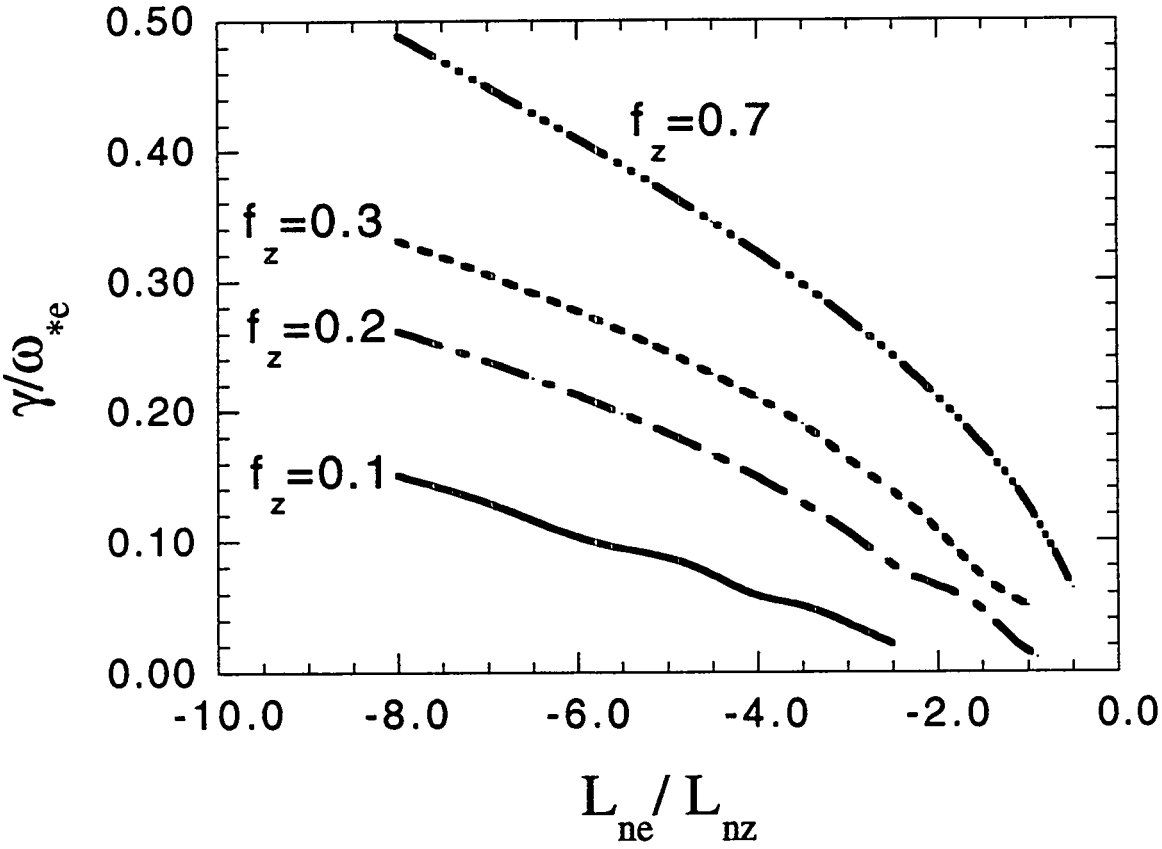
0.50
0.40
0.30
0.20
0.10
0.00
γ/ω*e
f z=0.7
f z=0.3
f z=0.2
f z=0.1
-10.0
-8.0
-6.0
-4.0
-2.0
0.0
L ne / L nz

Fig.2(b)

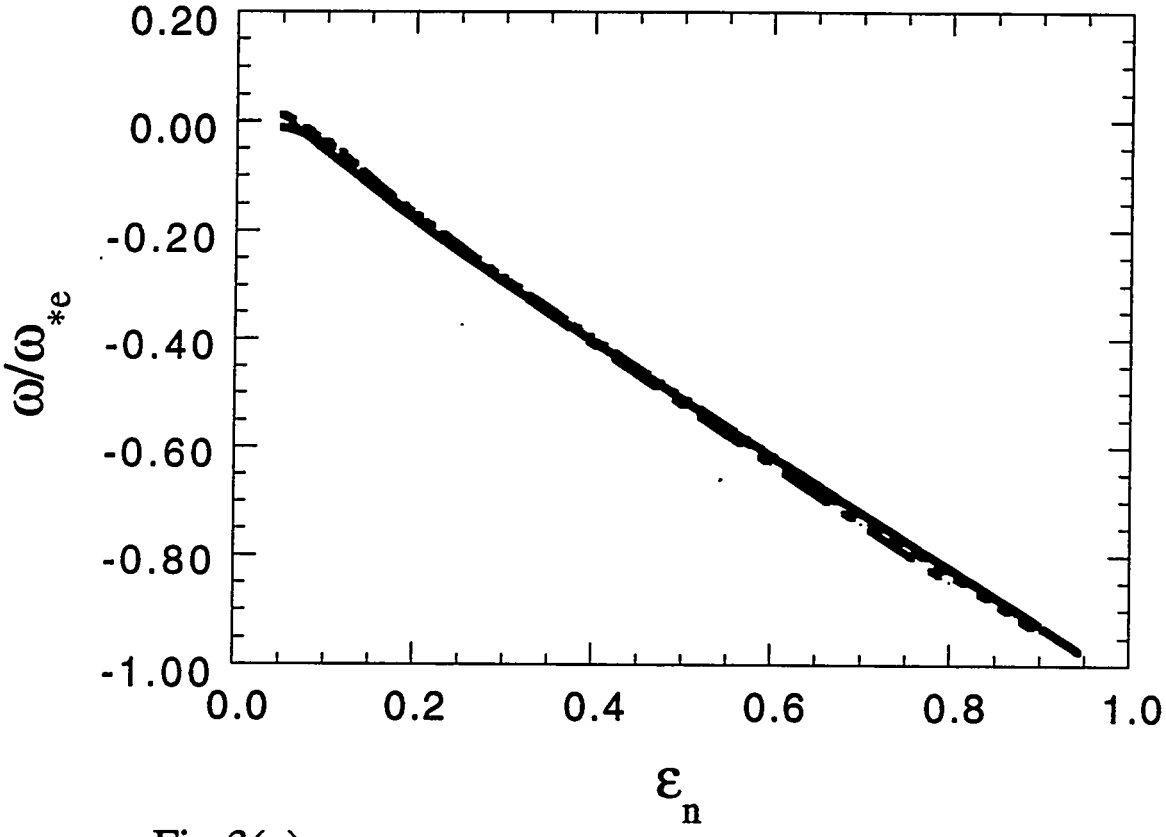

Fig.3(a)

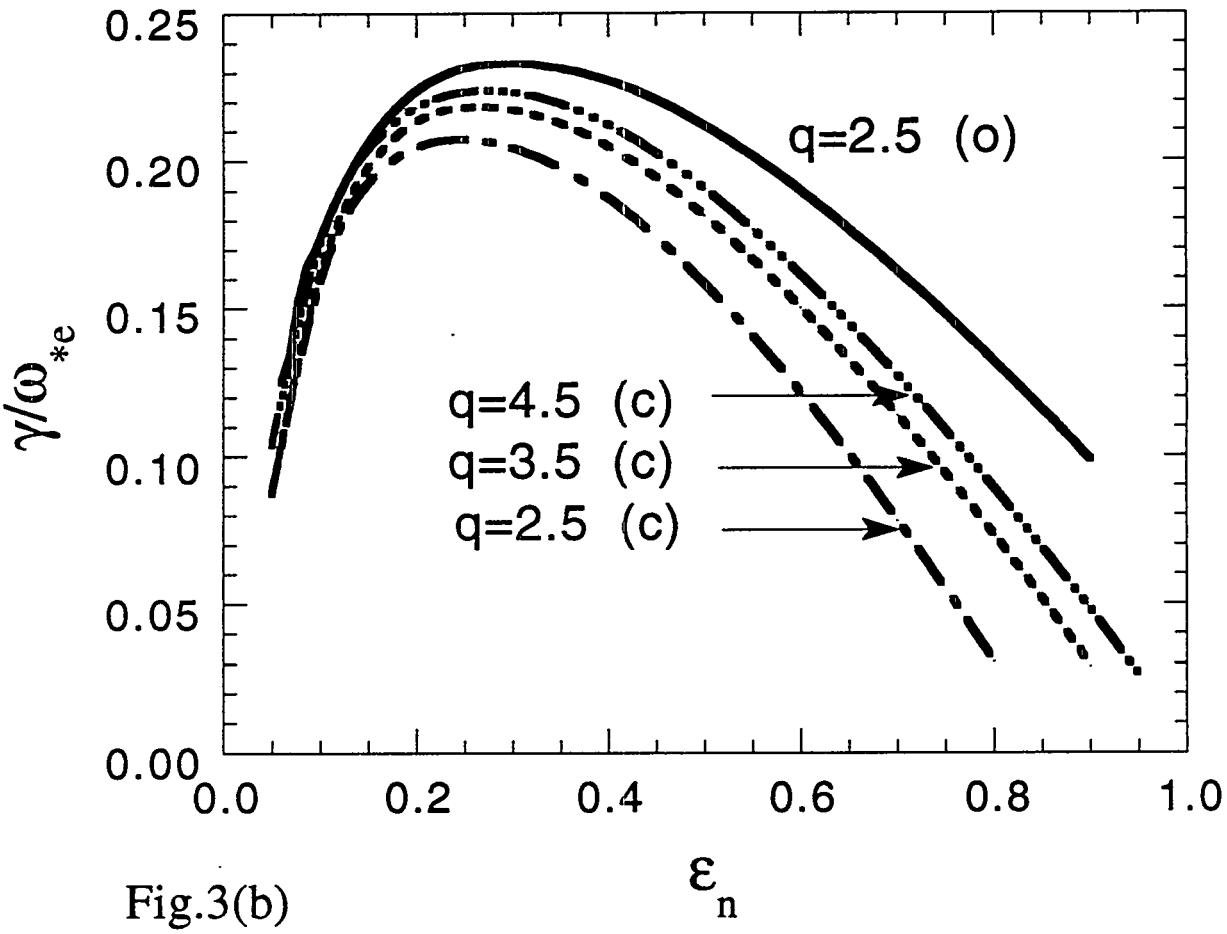
0.25
0.20
0.15
0.10
0.05
0.00
0.0
0.2
0.4
0.6
0.8
1.0
γ/ω*e
εn
q=2.5 (o)
q=4.5 (c)
q=3.5 (c)
q=2.5 (c)

Fig.3(b)

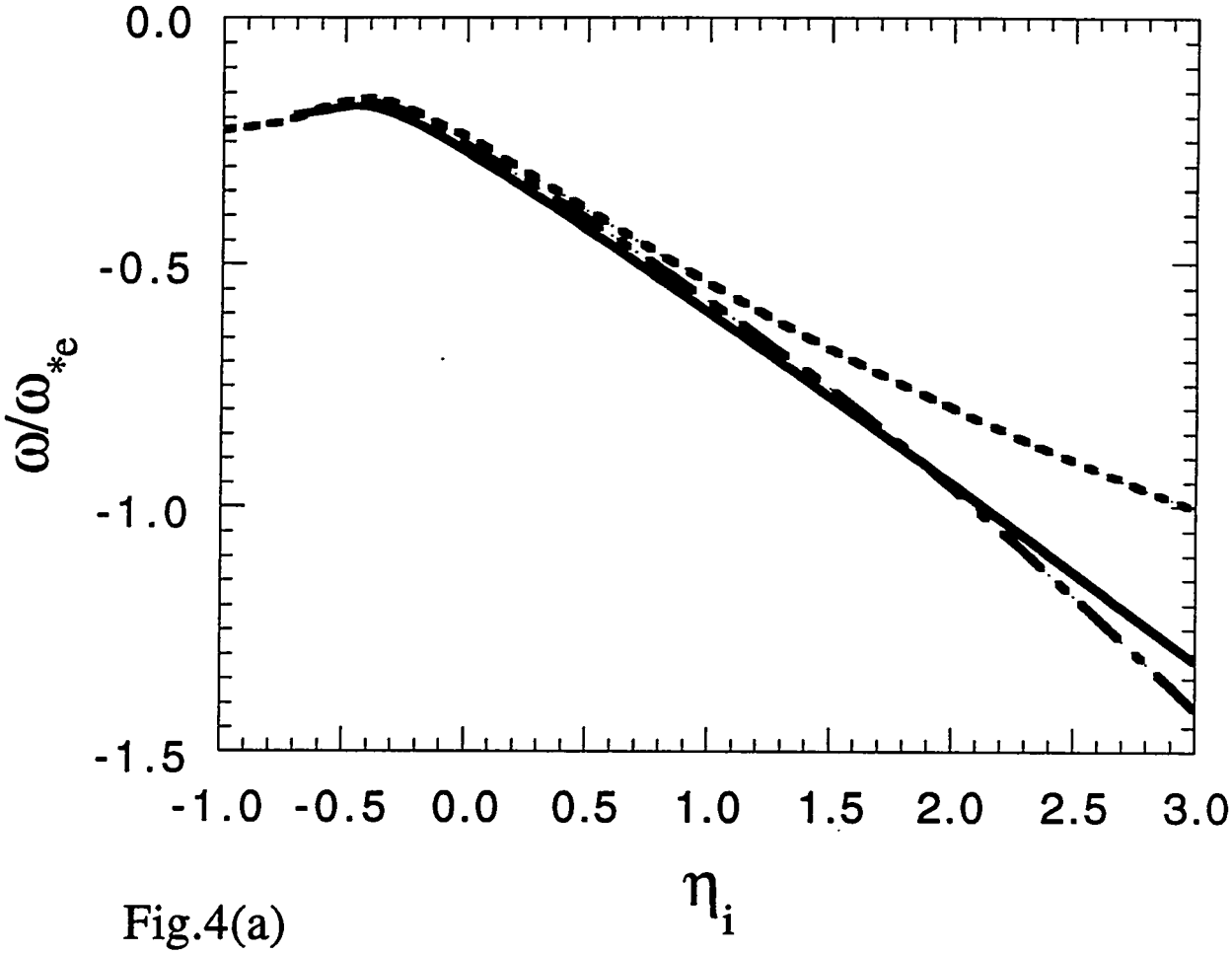

Fig.4(a)

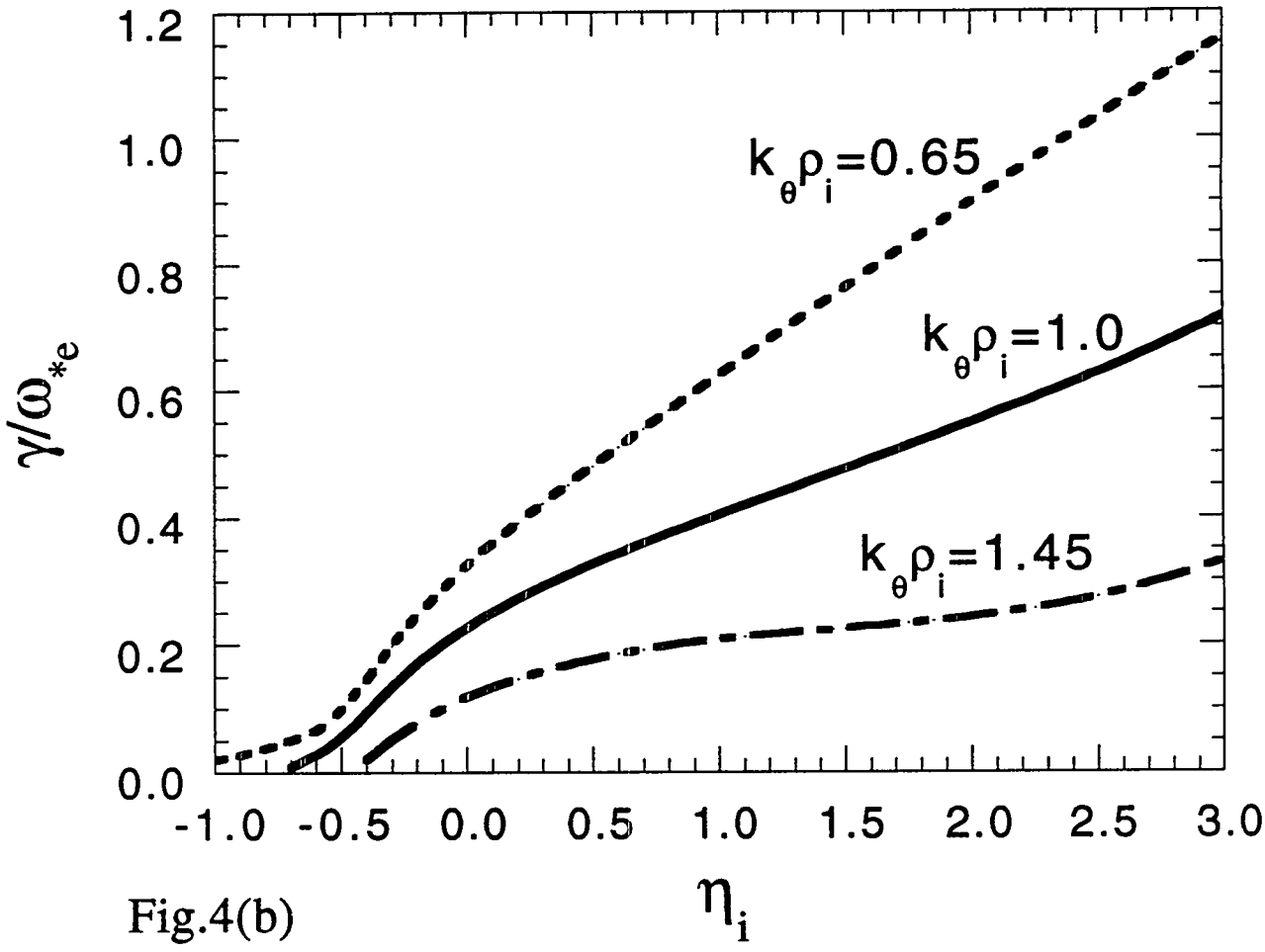
1.2
1.0
0.8
0.6
0.4
0.2
0.0
γ/ω_{*e}
$k_\theta\rho_i$=0.65
$k_\theta\rho_i$=1.0
$k_\theta\rho_i$=1.45
-1.0
-0.5
0.0
0.5
1.0
1.5
2.0
2.5
3.0
η_i

Fig.4(b)

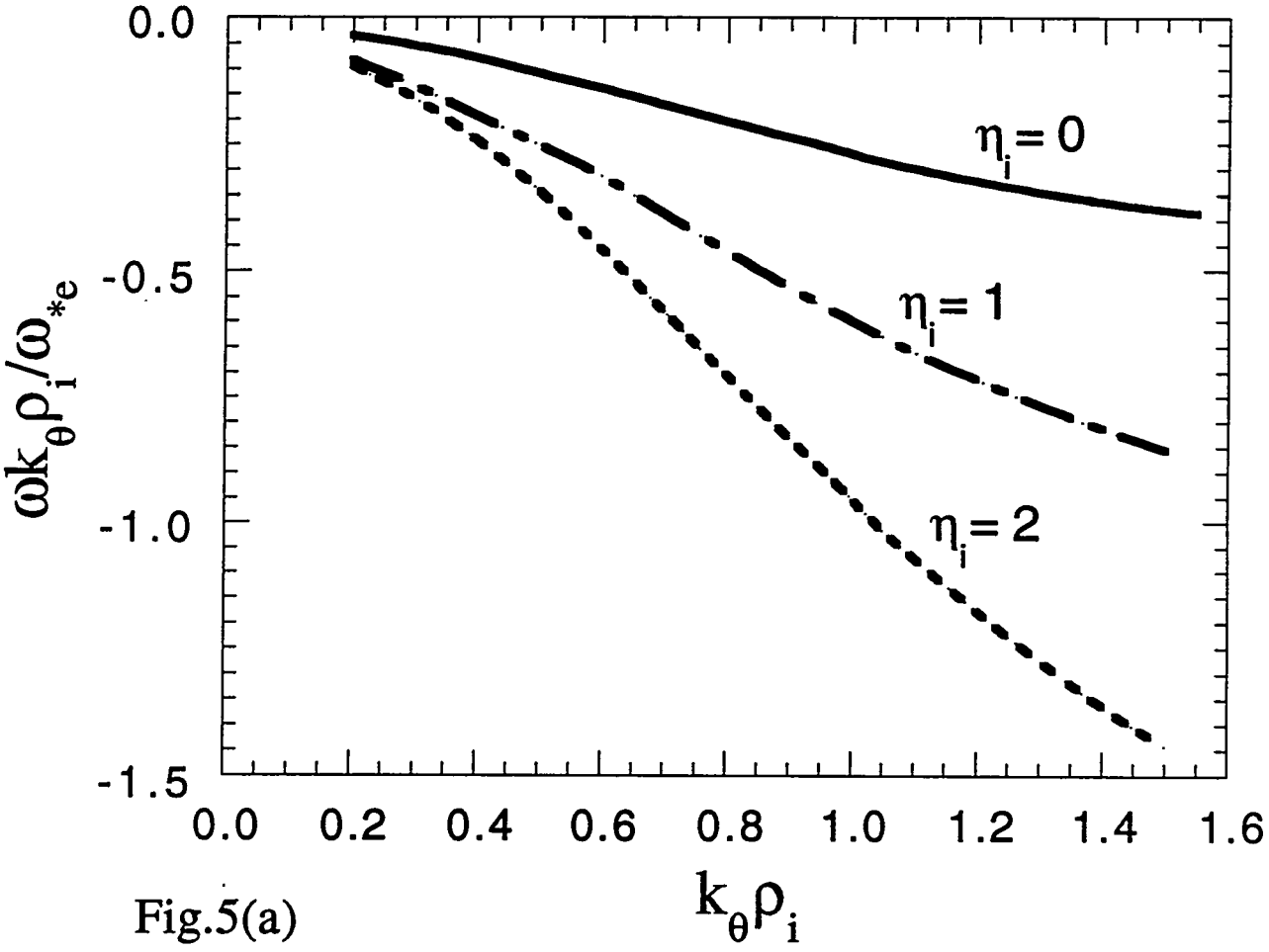
0.0
-0.5
-1.0
-1.5
0.0
0.2
0.4
0.6
0.8
1.0
1.2
1.4
1.6
$\omega k_\theta \rho_i / \omega_{*e}$
$k_\theta \rho_i$
$\eta_i = 0$
$\eta_i = 1$
$\eta_i = 2$

Fig.5(a)

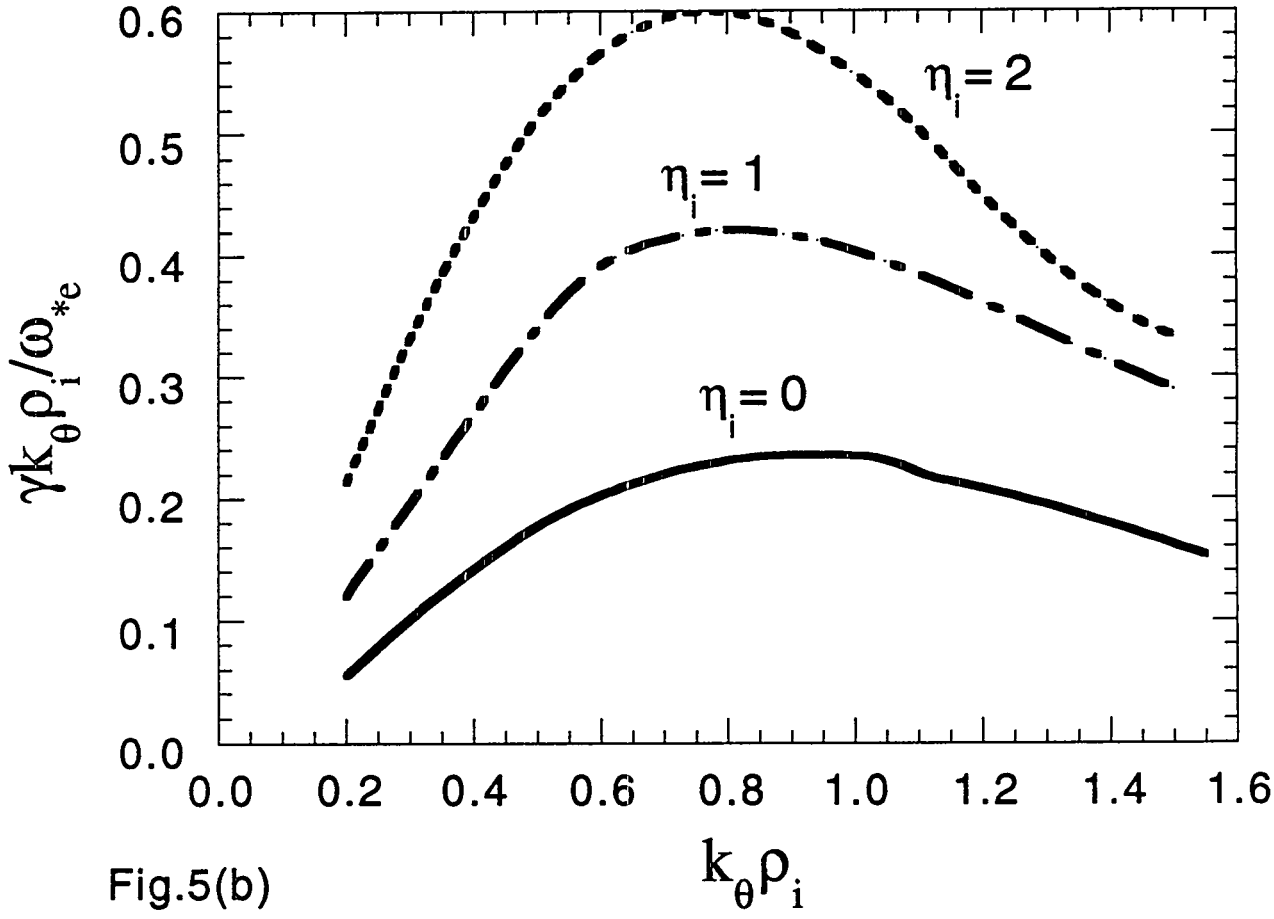
0.6
0.5
0.4
0.3
0.2
0.1
0.0
0.0
0.2
0.4
0.6
0.8
1.0
1.2
1.4
1.6
$\gamma k_\theta \rho_i / \omega_{*e}$
$k_\theta \rho_i$
$\eta_i = 2$
$\eta_i = 1$
$\eta_i = 0$

Fig.5(b)

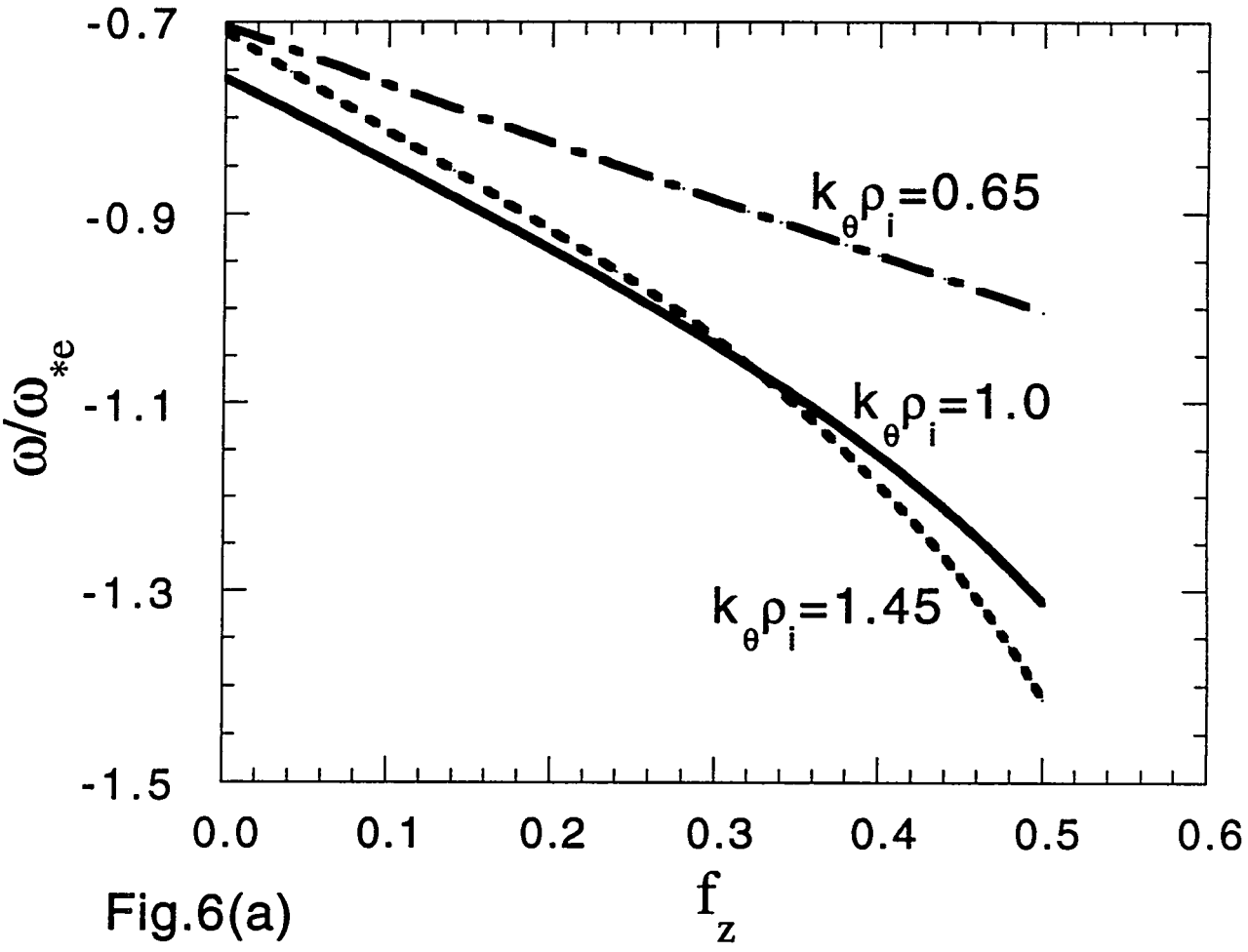

Fig.6(a)

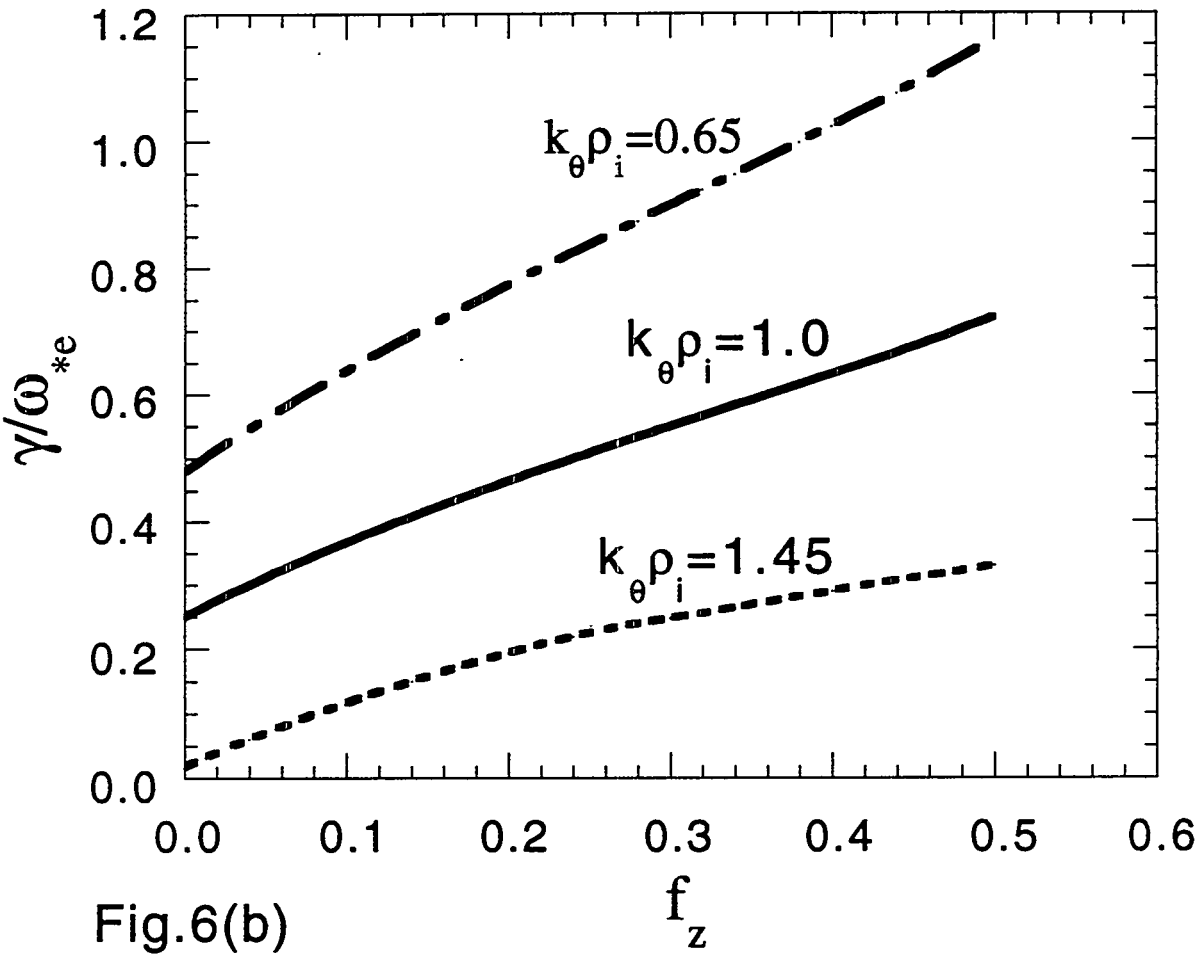
1.2
1.0
0.8
0.6
0.4
0.2
0.0
γ/ω_{*e}
$k_\theta\rho_i$=0.65
$k_\theta\rho_i$=1.0
$k_\theta\rho_i$=1.45
0.0
0.1
0.2
0.3
0.4
0.5
0.6
f_z

Fig.6(b)

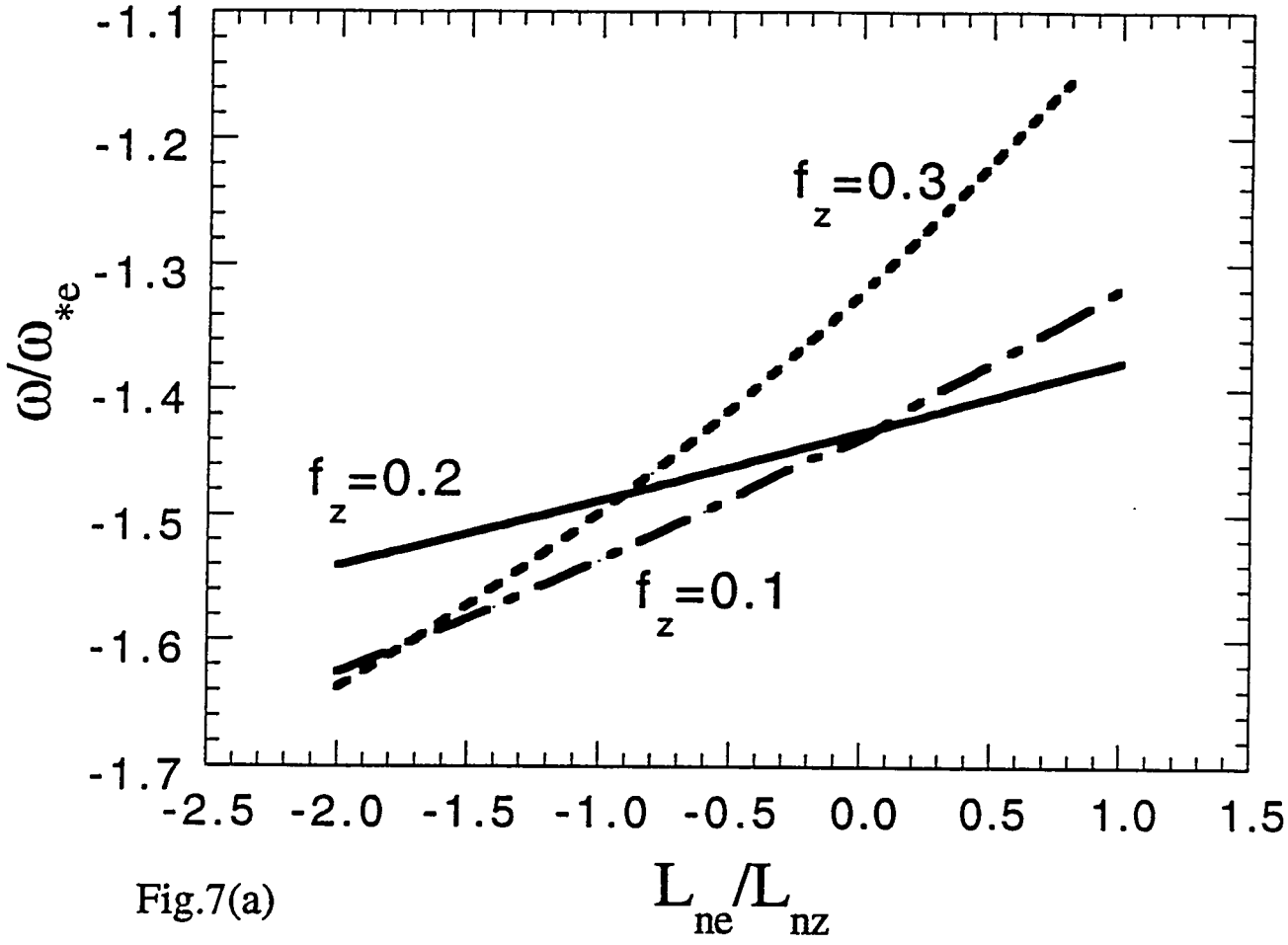
-1.1
-1.2
-1.3
-1.4
-1.5
-1.6
-1.7
ω/ω*e
f z=0.3
f z=0.2
f z=0.1
-2.5 -2.0 -1.5 -1.0 -0.5 0.0 0.5 1.0 1.5
Lne/Lnz

Fig.7(a)

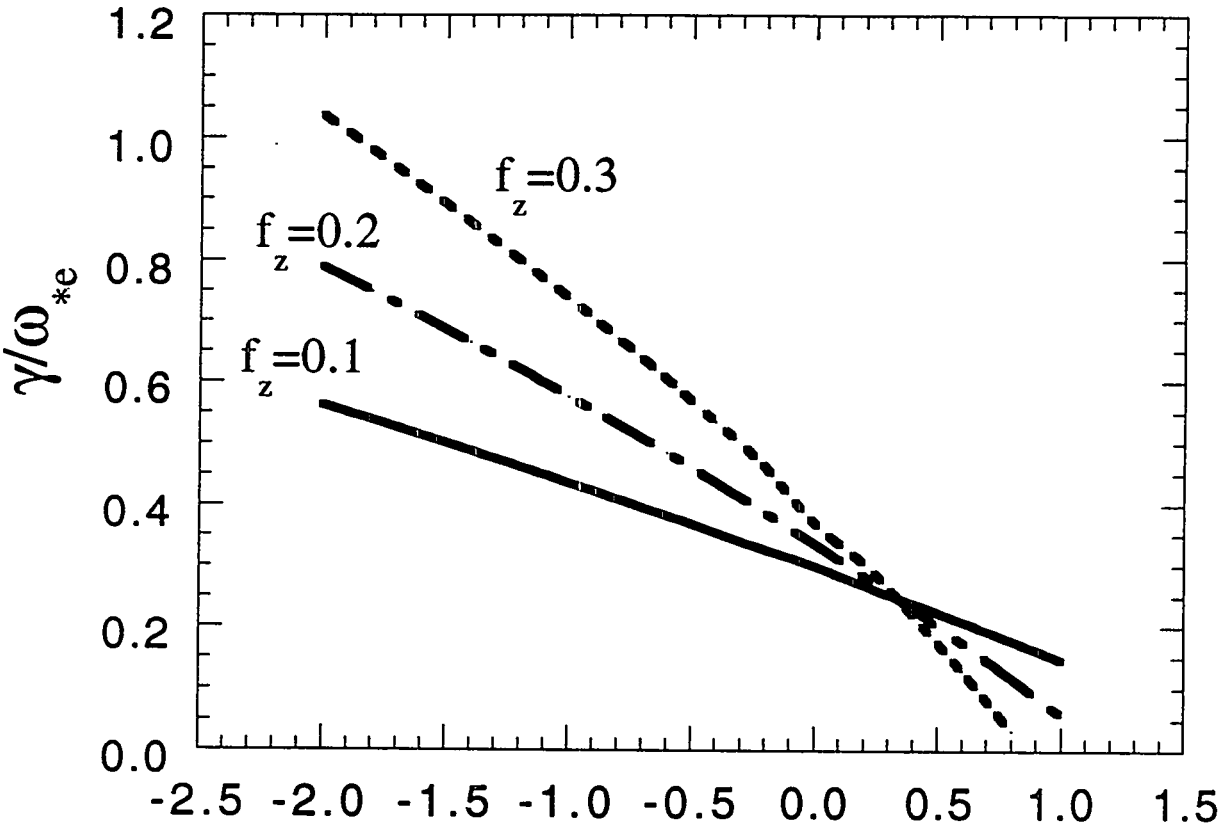
1.2
1.0
0.8
0.6
0.4
0.2
0.0
γ/ω_{*e}
f_z=0.3
f_z=0.2
f_z=0.1
-2.5 -2.0 -1.5 -1.0 -0.5 0.0 0.5 1.0 1.5
L_{ne}/L_{nz}

Fig.7(b)

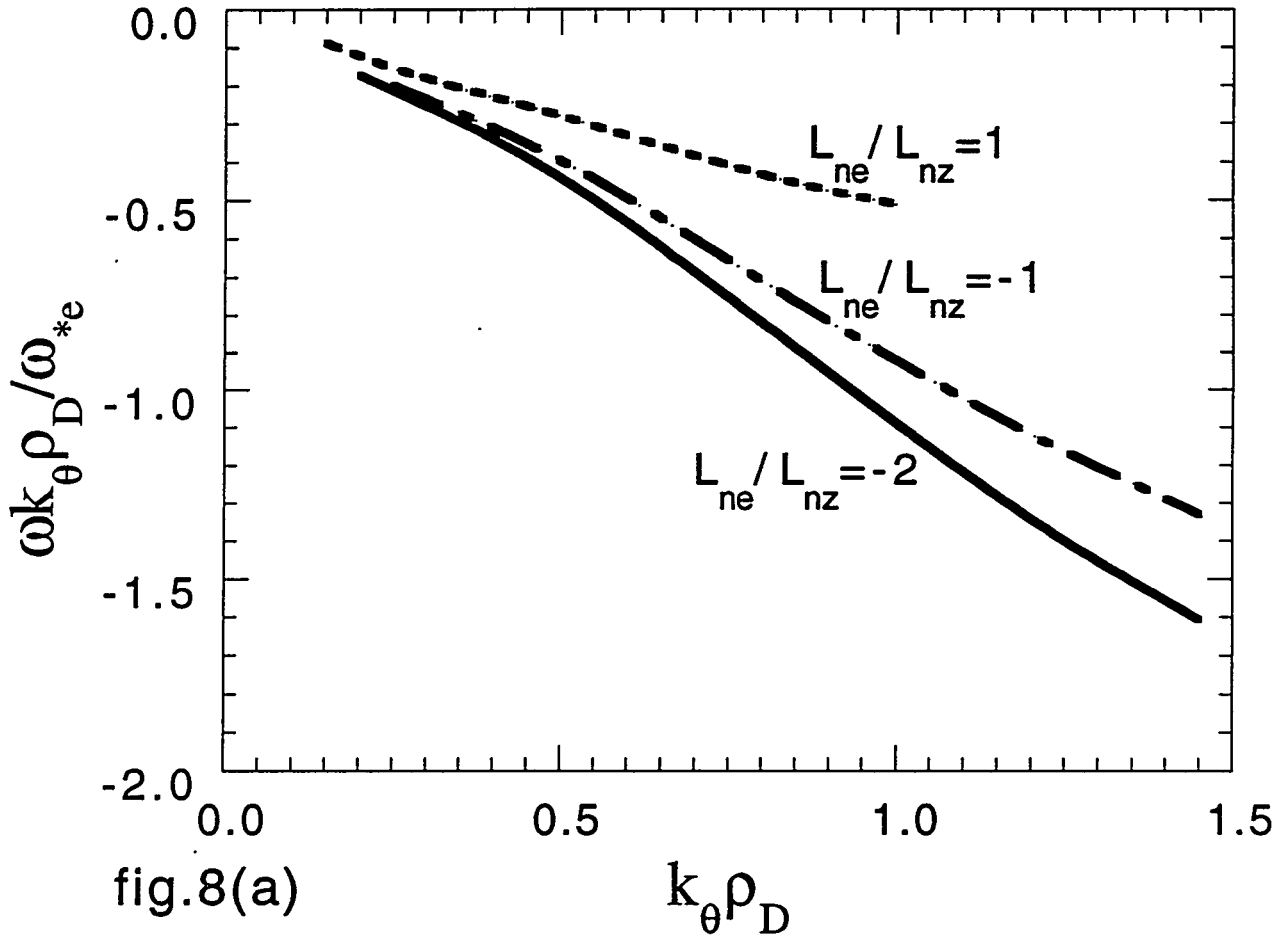
0.0
-0.5
-1.0
-1.5
-2.0
0.0
0.5
1.0
1.5
$\omega k_\theta \rho_D / \omega_{*e}$
$k_\theta \rho_D$
$L_{ne}/L_{nz}=1$
$L_{ne}/L_{nz}=-1$
$L_{ne}/L_{nz}=-2$

fig.8(a)

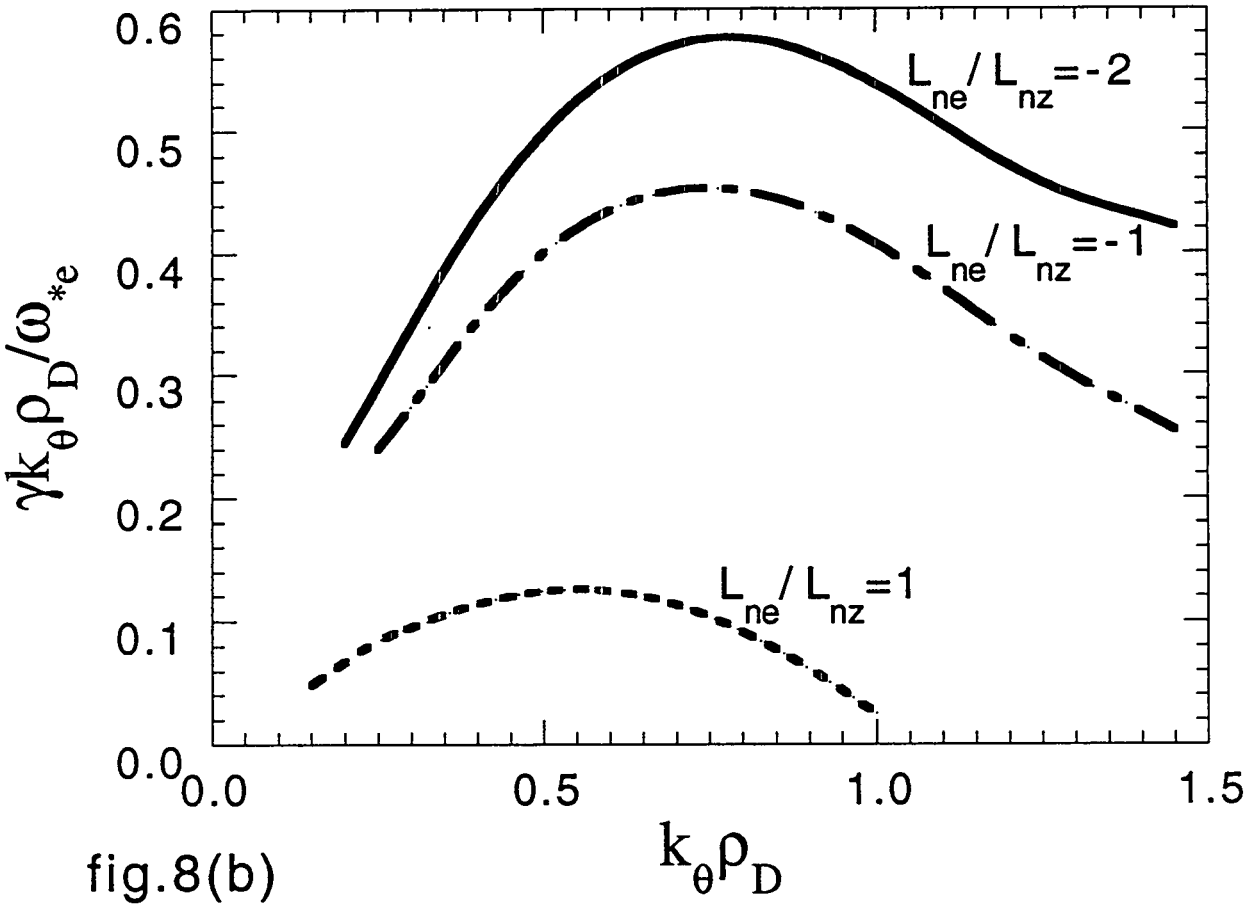
0.6
0.5
0.4
0.3
0.2
0.1
0.0
0.0
0.5
1.0
1.5
$\gamma k_\theta \rho_D / \omega_{*e}$
$k_\theta \rho_D$
$L_{ne}/L_{nz}=-2$
$L_{ne}/L_{nz}=-1$
$L_{ne}/L_{nz}=1$

fig.8(b)

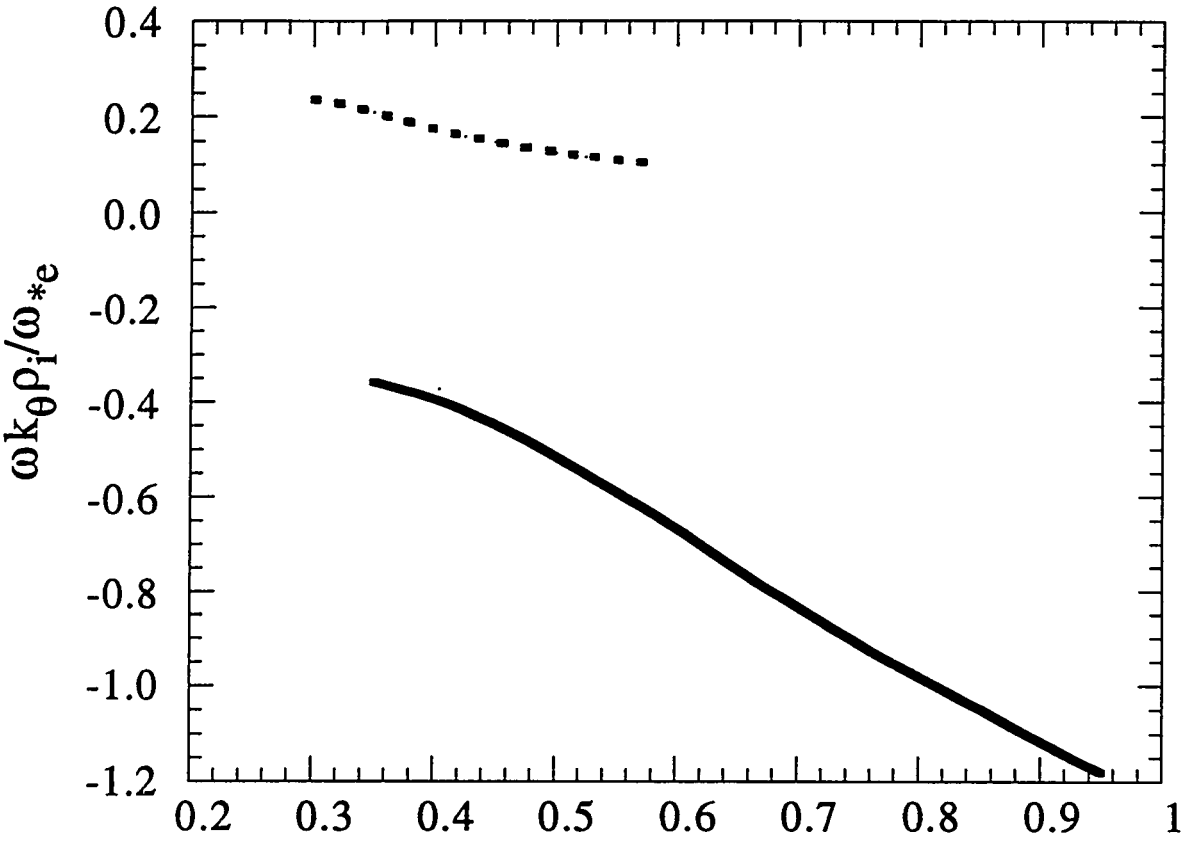
0.4
0.2
0.0
-0.2
-0.4
-0.6
-0.8
-1.0
-1.2
$\omega k_\theta \rho_i / \omega_{*e}$
0.2
0.3
0.4
0.5
0.6
0.7
0.8
0.9
1
$k_\theta \rho_i$

Fig.9(a)

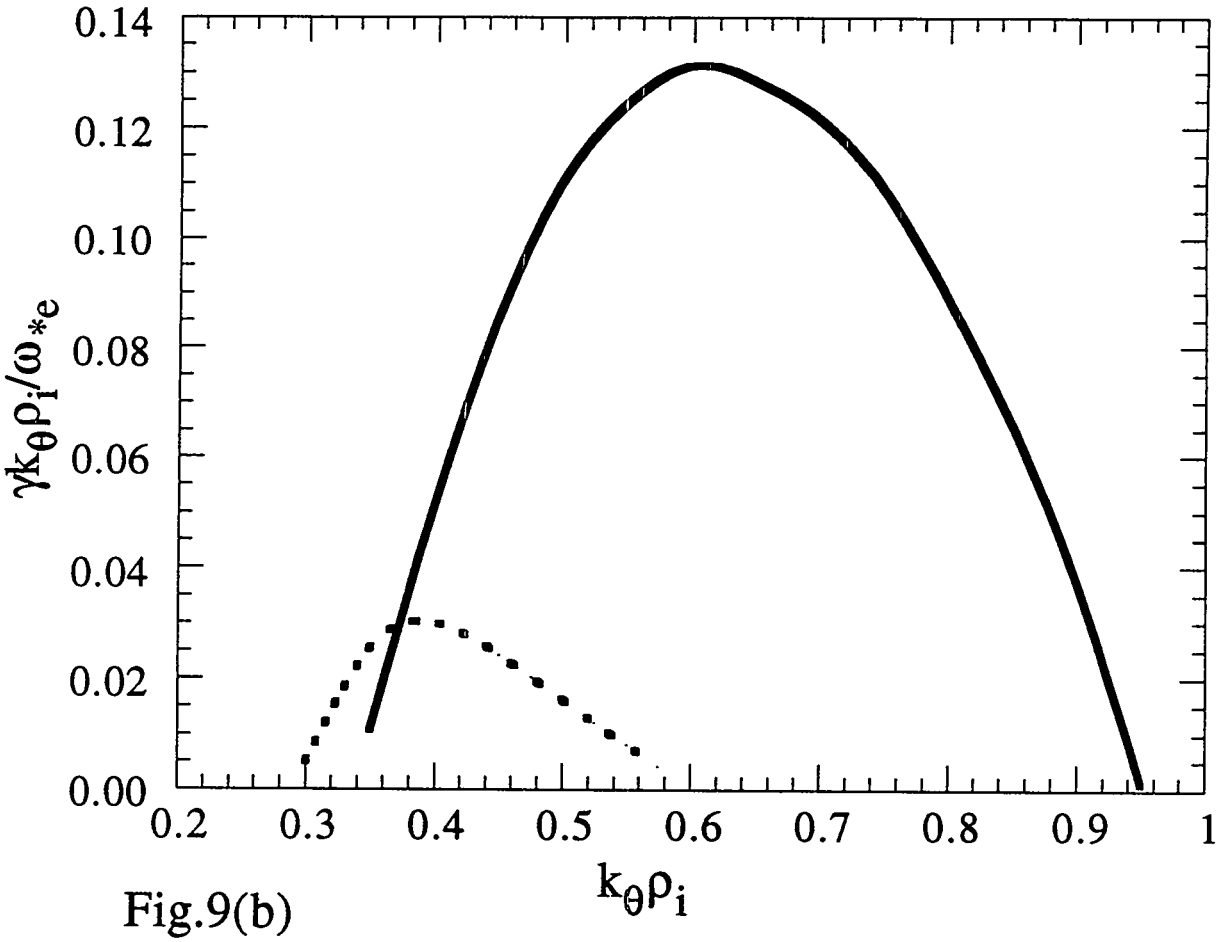
0.14
0.12
0.10
0.08
0.06
0.04
0.02
0.00
$\gamma k_\theta \rho_i / \omega_{*e}$
0.2
0.3
0.4
0.5
0.6
0.7
0.8
0.9
1
$k_\theta \rho_i$

Fig.9(b)

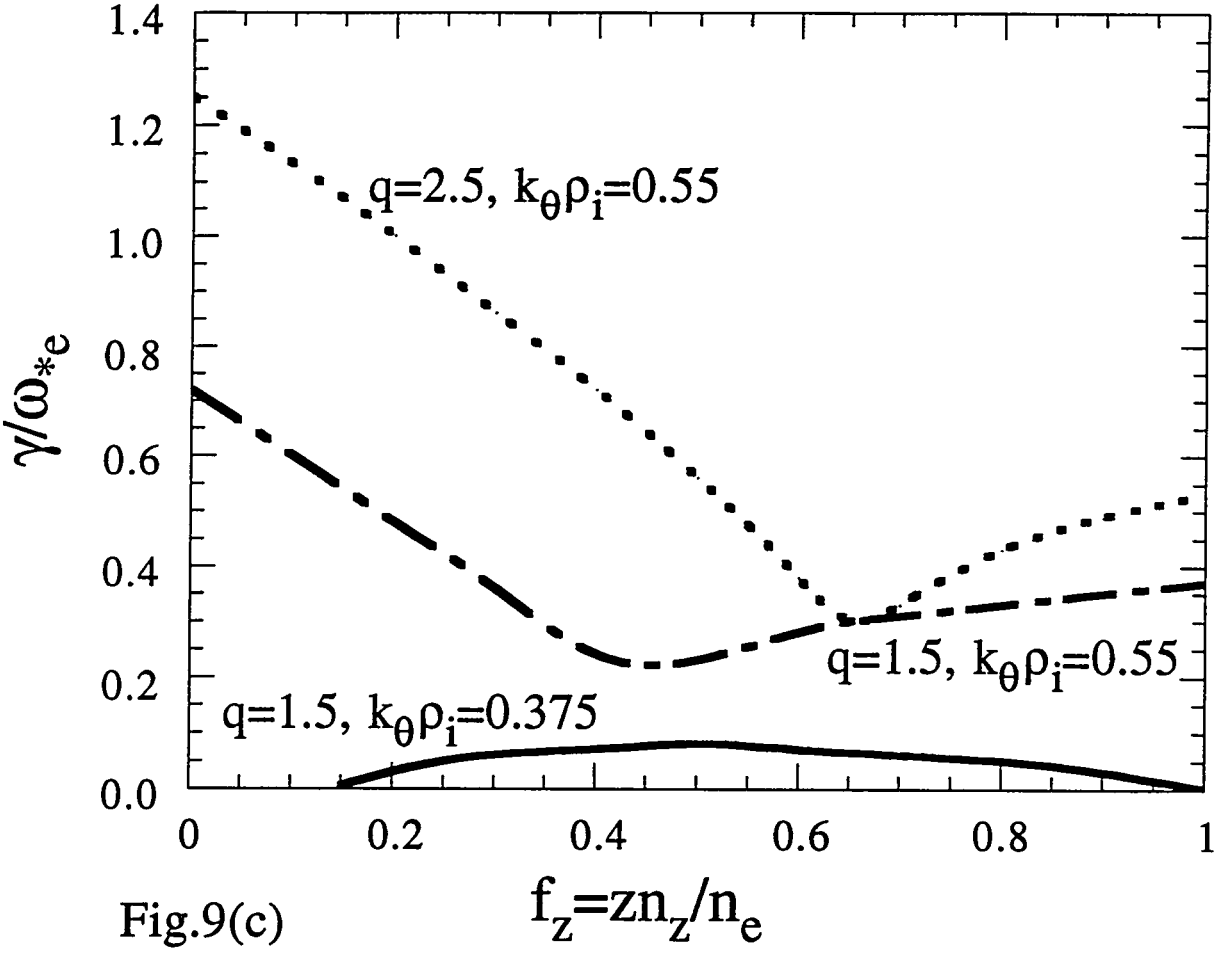
1.4
1.2
1.0
0.8
0.6
0.4
0.2
0.0
0
0.2
0.4
0.6
0.8
1
γ/ω*e
f_z=zn_z/n_e
q=2.5, k_θρ_i=0.55
q=1.5, k_θρ_i=0.55
q=1.5, k_θρ_i=0.375

Fig.9(c)